arXiv:1402.7175v1 [cond-mat.mes-hall] 28 Feb 2014

Rashba induced chirality switching of domain walls and suppression of the Walker breakdown

Martin Stier, Marcus Creutzburg, and Michael Thorwart
I. Institut für Theoretische Physik, Universität Hamburg, Jungiusstraße 9, 20355 Hamburg, Germany

In conventional domain wall systems the aim of a high domain wall velocity may be hindered by the occurrence of a Walker breakdown at comparably low current density. We show how a Rashba interaction can stabilize the domain wall dynamics and thereby shift the Walker breakdown to higher current densities. The Rashba interaction creates a field like spin torque, which breaks the symmetry of the system and modifies the internal structure of the domain wall. Besides a shift of the Walker breakdown it can additionally induce a chirality switch of the domain wall at sufficient Rashba fields. The preferred chirality may then be chosen by the direction of the current flow. Both, the suppression of the Walker breakdown and the chirality switching, affect the domain wall velocity. This is even more pronounced for short current pulses, where an additional domain wall movement after the pulse in either positive or negative direction can determine the final position of the domain wall.

PACS numbers: 75.78.Fg, 75.70.Tj, 75.25.-b

I. INTRODUCTION

Magnetic memory devices are based on the presence of microscopic magnetic domains where the alignment, or more precisely the alternation of alignments, of the magnetization stores the data. While in classical hard discs these domains are directly switched by a magnetic field, it is energetically far more efficient to push them through a wire by an electrical current[1–4]. The essence of this current induced domain wall (DW) motion is the interaction of the current's electron spins with the magnetic moments of the domains, resulting in a spin-transfer torque (STT). Two basic components of the STT arise in materials without a breaking of the symmetry in the electrons' subsystem: the adiabatic and the non-adiabatic STT[3,5]. The first STT stems from the adiabatic alignment of the electron spin and the magnetic moments, resulting in a DW motion due to total spin conservation. On the contrary, the latter, also known as the β-term, has its origin in a lag of the electron polarization behind the magnetic texture. Even though the non-adiabatic STT can lead to a considerable increase of the DW velocity with respect to the pure adiabatic motion, a very fast movement is limited by the Walker breakdown (WB) at a critical current density, which is accompanied by a precession of the magnetization[6] at the DW center. However this precession can be suppressed in systems of broken symmetry where a distinct direction of the magnetization or the electron spin is favored over the others. This may also imply a preference of a distinct chirality, or handedness, of the DW. For that matter Miron *et al.*[7] proposed the Rashba effect as a stabilizer of the DW chirality, resulting in a suppression of the WB and an increase of the DW velocity similar to the action of a transverse magnetic field[8,9]. In addition other symmetry breaking effects as the Dzyaloshinskii-Moriya interaction are supposed to enhance DW motion due to a preferred handedness[10–12]. By changing the thickness of layers of distinct materials the strength of the Dzyaloshinskii-Moriya interaction, and with it, the preferred chirality, can even be adjusted in certain limits[13].

The aim of this work is to reveal how a Rashba interaction acts on the chirality of a DW. We thereby consider the stabilization or destabilization of a distinct chirality in certain parameter regimes and their impact on the DW velocity. To do so, we set up a 1D model which allows us to calculate the STT including the induced Rashba field. By eventually solving the Landau-Lifshitz-Gilbert equation and hereby calculating DW velocities for opposite chiralities, we find several regimes of chirality-dependent DW motion in the according parameter limits. This actually includes the suppression of the WB but additionally a current-dependent switching to the preferred chirality. The optimal chirality can be chosen by the direction of the current flow. Results are presented in a broad parameter range including the current density, the strength of the Rashba interaction and current pulse lengths. Particularly for short current pulses the average DW velocity may differ strongly from the steady current value.

II. MODEL

We consider 1D wires in which the DWs are formed by localized magnetic moments $M_s\mathbf{n}(x,t)$ described by a unit vector $\mathbf{n}(x,t)$ and their saturation magnetization M_s. The actual shape of the DW is created by an effective magnetic field

$$\mathbf{H}_{\text{eff}} = -J_{\text{IA}}\partial_x^2\mathbf{n} - K_{\parallel}n_{\parallel}\mathbf{e}_{\parallel} + K_{\perp}n_{\perp}\mathbf{e}_{\perp} \ . \qquad (1)$$

Here the interaction strength J_{IA} is a measure for the magnetic moments to align parallel to each other, while the easy axis anisotropy $K_{\parallel}$ and the hard axis anisotropy $K_{\perp}$ are the energies of the respectively favorable or unfavorable directions for these moments. The explicit directions of these axes (e.g. x, y or z direction) have to be defined according to the situation which is present in

a distinct experimental setup. Even though the choice of the hard and easy axis is hardly of any importance in highly symmetric systems it becomes relevant if the symmetry is broken. Since this is the case for systems with a Rashba interaction we will consider different setups in this work.

The dynamics of the DW is governed by the Landau-Lifshitz-Gilbert equation

$$\partial_t \mathbf{n} = -\mathbf{n} \times \mathbf{H}_{\text{eff}} + \alpha \mathbf{n} \times \partial_t \mathbf{n} + \mathbf{T} \ , \tag{2}$$

which includes the effective field, the Gilbert damping α and an externally provided spin torque $\mathbf{T}$. In this work $\mathbf{T}$ has its origin in a spin polarized current interacting with the magnetic moments, thus being a spin transfer torque. To calculate this STT we set up a one-dimensional minimal model which describes the electron spins in a spin polarized current under the influence of a Rashba interaction. Its Hamiltonian consists of four parts according to

$$H = H_{\text{kin}} + H_{\text{sd}} + H_{\text{Rashba}} + H_{\text{relax}} \ , \tag{3}$$

with the kinetic energy, the *sd* and Rashba interaction as well as a relaxation part. As we only treat 1D system it is very convenient to use the 1D Sugawara representation of the Hamiltonian of the spin sector, since it (i) is a proper description for 1D systems[14] and (ii) provides a relatively simple and straightforward way to calculate the STT. The standard form of the kinetic part of the low energy Hamiltonian (in units of $\hbar = 1$, which we use from now on) is

$$H_{\text{kin}} = -iv \sum_{\sigma,p} \int dx c^\dagger_{p\sigma}(x) \partial_x c_{p\sigma}(x), \tag{4}$$

where $c^{(\dagger)}_{p\sigma}$ are the annihilators (creators) of electrons with spin $\sigma = \uparrow, \downarrow$ which are moving in the left or right direction ($p = L/R = -/+$). To rewrite this in the Sugawara form we define the spin density operators[15]

$$\mathbf{J}_p(x) = \frac{1}{2} : c^\dagger_{p\sigma}(x) \boldsymbol{\sigma}_{\sigma\sigma'} c_{p\sigma'}(x) : \tag{5}$$

with the Pauli matrices $\boldsymbol{\sigma}$ and the colons $: \cdots :$ denoting normal ordering. The Hamiltonian now reads

$$H_{\text{kin}} = v \sum_p \int dx \ : \mathbf{J}_p \cdot \mathbf{J}_p : + H_{\text{charge}} \tag{6}$$

with an irrelevant charge part[16]. The introduction of spin density operators for left and right moving particle allows for a simple definition of the total spin density

$$\mathbf{s} = \mathbf{J}_R + \mathbf{J}_R \tag{7}$$

and, more importantly, of the spin current density

$$\mathbf{J} = v(\mathbf{J}_R - \mathbf{J}_L) \ , \tag{8}$$

which reduces to a vector instead of a tensor in 1D. All remaining parts of the total Hamiltonian (3) can also be expressed in terms of the $\mathbf{J}_p$. This is obvious for the *sd* Hamiltonian

$$H_{\text{sd}} = \Delta_{\text{sd}} \int dx \ \mathbf{s} \cdot \mathbf{n} = \Delta_{\text{sd}} \sum_p \int dx \ \mathbf{J}_p \cdot \mathbf{n} \ , \tag{9}$$

while a similar form can be achieved for H_{Rashba} with some simplifications in strict 1D quantum wires. The conventional Rashba Hamiltonian

$$H_{\text{Rashba}} = \tilde{\alpha}_R (k_x \sigma_y - k_y \sigma_x) \tag{10}$$

reflects motion in 2D, while we may neglect the movement in one of the directions in 1D wires. Thus we only keep $H_{\text{Rashba}} = \tilde{\alpha}_R k_x \sigma_y$ for our calculations, which ignores some higher order mixing of states[17]. Additionally in a low-energy model only wave vectors in the vicinity of the Fermi wave vector k_F are relevant and we can replace $k_x \to k_F$ for right moving and $k_x \to -k_F$ for left moving particles. This yields the simplified Rashba Hamiltonian

$$H_{\text{Rashba}} = \Delta_{\text{R}} \sum_p p \int dx \ \mathbf{J}_p \cdot \mathbf{e}_y, \quad \Delta_{\text{R}} = 2\tilde{\alpha}_R k_F. \tag{11}$$

For simplicity we combine the two interactions to

$$\begin{aligned} H_{\text{IA}} \equiv & H_{\text{sd}} + H_{\text{Rashba}} \\ = & \Delta_{\text{sd}} \sum_p \int dx \ \mathbf{J}_p \cdot \mathbf{m}_p \end{aligned} \tag{12}$$

$$\mathbf{m}_p = \mathbf{n} + p\alpha_R \mathbf{e}_y \tag{13}$$

and introduce a reduced Rashba interaction $\alpha_R = \Delta_{\text{R}}/\Delta_{\text{sd}}$.

The last part of the total Hamiltonian (3) is the relaxation part, which we only define implicitly by the help of the commutator

$$-i \left[\mathbf{J}_p, H_{\text{relax}}\right]_- = \frac{1}{\tau}(\mathbf{J}_p - \mathbf{J}^{\text{relax}}_p) \ . \tag{14}$$

Even though this relaxation time approximation (with the relaxation time τ) can be justified by a microscopic Hamiltonian, we will not do it here but refer to Ref. 18 for further details.

A. Equation of motion

Next, we formulate the equation of motion (EOM) of $\mathbf{J}_p$ by calculating

$$\partial_t \mathbf{J}_p = -i \left[\mathbf{J}_p, H\right]_- \ . \tag{15}$$

This will eventually yield the STT

$$\mathbf{T} = -\Delta_{\text{sd}} \mathbf{n} \times \mathbf{s} = -\Delta_{\text{sd}} \mathbf{n} \times \sum_p \mathbf{J}_p \ . \tag{16}$$

Keeping in mind that the spin density operators in the low-energy description follow a Kac-Moody-Algebra[15]

$$\left[J_p^\mu(x), J_{p'}^\nu(x')\right]_- = i[p\partial_x + \epsilon^{\mu\nu\lambda}J_p^\lambda]\delta_{pp'}\delta(x-x'), \quad (17)$$

we find

$$(\partial_t + vp\partial_x)\mathbf{J}_p = -\Delta_{\rm sd}[\mathbf{J}_p \times \mathbf{m}_p + \beta(\mathbf{J}_p - \mathbf{J}_p^{\rm relax})], \quad (18)$$

where we have defined $\beta = (\Delta_{\rm sd}\tau)^{-1}$. The explicit choice of the relaxation state is crucial for the resulting STT, since it not only changes the values of the equation but also influences the symmetry of the system. As it is shown by van der Bijl *et al.*[19], this actually affects the existence of distinct STTs. We will determine $\mathbf{J}_p^{\rm relax}$ by a specific requirement formulated below. To actually solve the EOM (18) we apply a gradient expansion scheme. We express $\mathbf{J}_p$ in orders of derivatives of $\mathbf{m}_p$ as

$$\mathbf{J}_p = \mathbf{J}_p^{(0)}(\mathbf{m}_p) + \mathbf{J}_p^{(1)}(\partial_x\mathbf{m}_p, \partial_t\mathbf{m}_p) + \dots \ . \quad (19)$$

Note that obviously $\partial_{x,t}\mathbf{m}_p = \partial_{x,t}\mathbf{n}$. The combination of the Ansatz (19) and the EOM (18) allows for an arrangement by the orders on the according left and right hand side of the equation as

$$\begin{aligned} 0 &= -\Delta_{\rm sd}[\mathbf{J}_p^{(0)} \times \mathbf{m}_p - \beta(\mathbf{J}_p^{(0)} - \mathbf{J}_p^{\rm relax})] \\ (\partial_t + vp\partial_x)\mathbf{J}_p^{(0)} &= -\Delta_{\rm sd}[\mathbf{J}_p^{(1)} \times \mathbf{m}_p - \beta(\mathbf{J}_p^{(1)} - 0)] \\ \cdots &= \dots \ . \end{aligned}$$

Starting from zeroth order we can now solve the equation successively to, in principle, arbitrary order. Since higher order terms become very involved, we restrict the calculation to zeroth and first order in this work.

Up to now we have not defined the relaxation state explicitly. Typical choices in literature let the electron spin either relax towards the direction of the magnetization[20] ($\mathbf{J}_p^{\rm relax} \propto \mathbf{n}$) or to the combined vector[19] $\mathbf{J}_p^{\rm relax} \propto \mathbf{m}_p$. We fix the actual $\mathbf{J}_p^{\rm relax}$ by the requirement that it is a solution of the EOM (18), at least in zeroth order. This means that the system can *actually* relax into that state far away from the DW center. Putting $\mathbf{J}_p^{(0)} = \mathbf{J}_p^{\rm relax}$ into the zeroth order part of the EOM yields

$$\mathbf{J}_p^{\rm relax} \propto \mathbf{m}_p \ , \quad (20)$$

while, for instance, a relaxation $\propto \mathbf{n}$ is not possible under the requirement that the system can arrive at $\mathbf{J}_p^{\rm relax}$. It follows immediately that $\mathbf{J}_p^{(0)} = \mathbf{J}_p^{\rm relax}$ is the only solution for zeroth order and we set

$$\mathbf{J}_p^{\rm relax} = j_p\frac{\mathbf{m}_p}{|\mathbf{m}_p|}, \quad (21)$$

with some constants $j_{L/R}$ representing the spin density of the left/right movers. Finally we define the spin current density I_s as

$$I_s^2 \equiv (\mathbf{J}^{(0)})^2 = \sum_{p,p'} pp'\frac{j_p}{|\mathbf{m}_p|}\frac{j_{p'}}{|\mathbf{m}_{p'}|}\mathbf{m}_p\mathbf{m}_{p'} \ . \quad (22)$$

Far away from the DW center ($n_y = 0$), we have

$$I_s^2 \equiv (\mathbf{J}^{(0)})^2 = \sum_{p,p'} v^2\left(p\frac{j_p}{|\mathbf{m}_p|} + \alpha_R^2\frac{j_p}{|\mathbf{m}_p|}\right) \ . \quad (23)$$

The second term in Eq. (23) is connected to the evolving spin density but has no contribution to the net spin current. Hence, we can neglect this part. Thus we find the simple result for the spin current density as

$$I_s = v(\frac{j_R}{|\mathbf{m}_R|} - \frac{j_L}{|\mathbf{m}_L|}), \quad (24)$$

which is connected to the definition of spin currents in Eq. (8). Fortunately, it is not necessary to know the particular values of $j_{R/L}$ as they will only appear in the combination of Eq. (24) in the expressions for the STT. Thus, the relation (24) is sufficient to calculate the STT. For an easier comparison with experimental data this spin current density may be written as $I_s = PI_c/(2e)$ where P is the spin polarity, e the elementary charge and I_c the charge current density of a spin polarized current.

B. Spin torque

The solutions of Eq. (18) yield the STT according to $\mathbf{T}^{(0,1)} = -\Delta_{\rm sd}\mathbf{n}\times\sum_p \mathbf{J}_p^{(0,1)}$ in zeroth and first order. For zeroth order we get a field-like term

$$\mathbf{T}_1^{(0)} = -\mathbf{n}\times\left[I_s\frac{\alpha_R(1+\alpha_R^2)}{\mathcal{N}}\frac{\Delta_{\rm sd}}{v}\mathbf{e}_y\right] \equiv -\mathbf{n}\times\mathbf{H}_R^{(0)}, \quad (25)$$

with $\mathcal{N} = (1+\alpha_R^2)^2 - 4\alpha_R^2 n_y^2$. Note that we do not get a Sloncezwksi-like field torque as $\mathbf{T}^{\rm Sl} = \beta\mathbf{n}\times(\mathbf{n}\times\mathbf{H}_R^{(0)})$ which is due to our choice of $\mathbf{J}_p^{\rm relax}$. A different direction of $\mathbf{J}_p^{\rm relax}$ (and with it a different symmetry of the system), e.g. $\mathbf{J}_p^{\rm relax} \propto \mathbf{n}$, would yield such a $\mathbf{T}^{\rm Sl}$ in our approach, as well[21].

However, the field-like term is of major importance in Rashba systems as it does not appear for $\alpha_R = 0$ and results in new behavior of the DW dynamics. In contrast to that, the typical first order adiabatic and non-adiabatic STTs are only affected via a renormalization of α_R as

$$T_{\rm ad}^{(1)} = -I_s\frac{1+\alpha_R^2(1-2n_y^2)}{\mathcal{N}}\partial_x\mathbf{n}, \quad (26)$$

$$T_{\rm non-ad}^{(1)} = \beta I_s\frac{1+\alpha_R^2}{\mathcal{N}}\mathbf{n}\times\partial_x\mathbf{n} \ . \quad (27)$$

Particularly for small α_R this renormalization plays a minor role. More important is a non-adiabatic first-order correction to the Rashba field which reads

$$\mathbf{H}_R^{(1)} = I_s\beta\partial_x n_y\alpha_R^2\frac{1+\alpha_R^2(1+4n_y^2)}{\mathcal{N}^2}. \quad (28)$$

This term may become large for steep DWs with a large derivative $\partial_x n_y$. Thus the total Rashba field up to first

order is given as

$$\mathbf{H}_R = I_s \left[\frac{\alpha_R(1+\alpha_R^2)}{\mathcal{N}} \frac{\Delta_{\rm sd}}{v} + \beta \partial_x n_y \frac{\alpha_R^2 + \alpha_R^4(1+4n_y^2)}{\mathcal{N}^2} \right] \mathbf{e}_y \ . \quad (29)$$

Additional terms $\mathbf{T}_t \propto \partial_t \mathbf{n}$ also appear, which renormalize the Gilbert damping α. As the origin of α, and with it, the dependence on other parameters is not very well established in theory, we will neglect all torques $\propto \partial_t \mathbf{n}$ to get a constant model parameter α for all calculations. This allows for a better comparison of the results.

III. RESULTS

In 1D systems we theoretically have the freedom of choice for the directions of the easy and hard axes, the direction of the Rashba field and the chirality of the DW. We will consider systems which always have the easy axis in z direction while the Rashba field points in y direction. At the respective ends of the wire, we set $n_z(x \to \pm\infty) = \pm 1$ as boundary conditions to solve the Landau-Lifshitz-Gilbert equation numerically. A crucial point of this work is the effect of the direction of the hard axis and the initial chirality of the DW on its dynamics. We will show results for four types of DWs: the hard axis in x or y direction and a positive or negative chirality $C = \pm 1$. Chirality is defined as the clockwise ($C = +1$) or the counter-clockwise ($C = -1$) rotation of the magnetic moment in the according plane. For our system an initial direction sense of the magnetic moment $n_{x(y)} > 0$ at the DW center for hard y (x) axis means a negative chirality and vice versa.

As model parameters we choose dimensionless values which correspond to the estimated values[22] of Ta/CoFeB/MgO when we measure the length (time) in units of $x_0 = 0.5$nm ($t_0 = 1$ps). We have: $J = 5.2$, $K_\parallel = 0.185$, $K_\perp = 0.008$, $\alpha = \beta = 0.06$. In addition we set $\Delta_{\rm sd}/v = 0.2$, $v = 400$ and the polarity of the spin current $P = 1$.

The DW center $x_{\rm DW}$ is defined by the requirement that $n_z(x_{\rm DW}) = 0$ and the DW velocity as $v_{\rm DW} = \partial_t x_{\rm DW}$.

A. Chirality switching

In systems without any symmetry breaking, all of the four configurations ($C = \pm 1$, hard axis in x or y direction), are equivalent with respect to the DW dynamics. This changes when a Rashba interaction is present. Then, the Rashba field $\mathbf{H}_R$, pointing in y direction in this work, is the decisive quantity. The basic reasons for that can be easily understood when we look at the finite magnetic component at the DW center $x_{\rm DW}$. As we consider Bloch(z) walls, the z component $n_z(x_{\rm DW})$ is always zero.

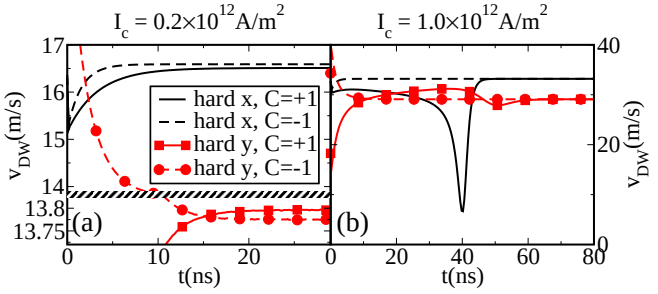

FIG. 1. (Color online) DW velocity vs time for hard axis anisotropy in x and y direction and initial chirality $C = +1$ (solid lines) and $C = -1$ (dashed) and current densities as indicated within the plot. For small current densities (a) a small but finite velocity difference $\Delta v_{\rm DW} = v_{\rm DW}^{C=-1} - v_{\rm DW}^{C=+1}$ exists for all times (mind the magnified y axis below the hatched area). In contrast to that, velocities become equal at a sufficient critical Rashba field $H_R \propto I_c \alpha_R$ (b). This is accompanied by a switching to the optimal chirality at $t \approx 40$ ns (hard x) or $t \approx 60$ ns (hard y), respectively. Parameter: $\alpha_R = 0.3$, (for the remaining parameters see text).

In addition, the hard axis defines the second vanishing component, and with it, the only remaining finite one, as it always holds $\mathbf{n}^2 = 1$. For a hard axis in x direction there is a finite component only in the y direction, which means that $\mathbf{H}_R$ couples parallel to the magnetization, while it is perpendicular to $\mathbf{n}(x_{\rm DW})$ for a hard y axis. Note that in our approach, where $\mathbf{H}_R$ includes the derivative of the magnetization $\partial_x n^y$, the choice of the hard axis additionally has an direct effect on the Rashba field itself, as $\partial_x n^y$ would vanish (at least initially) for a hard axis in y direction. In addition, the chirality defines the sign of the finite component. While the anisotropy field couples quadratically (with no preference of a sign of $\mathbf{n}$) to the magnetization, the Rashba field enters as a linear term. Thus $\mathbf{H}_R$ prefers a distinct sign of the magnetization, and with it, distinct chiralities.

A chirality-sensitive motion has been already addressed in the literature[23] where the Rashba interaction acts similarly as the β term (non-adiabatic torque) where the sign of this term actually depends on the chirality. Different to our approach, the precession and, with it, a change of the chirality were not considered in Ref. 23.

Figure 1 shows the difference in velocity of the DW for both: (i) different hard axes and (ii) different chiralities. For small currents I_c, the velocities of $C = \pm 1$ differ for all times t. This changes if $\mathbf{H}_R$ exceeds a critical value. Even though the velocities still start at distinguished values they finally match after some time and stay the same. In an *ideal long term* average the movement of both chiralities would appear exactly equally. Similar results have been found for vortex DWs in magnetic nanotubes with an externally applied magnetic field[24].

The approach of both velocities is accompanied by a switching of the sense of the magnetization, as it is shown in Fig. 2. As soon as $\mathbf{H}_R$ is strong enough to overcome $K_\perp$ it will rearrange the magnetization to its optimal ori-

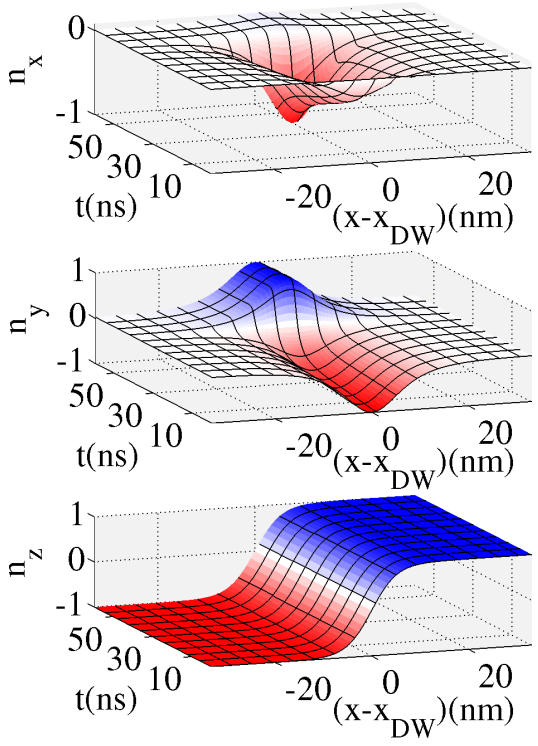

FIG. 2. (Color online) Components of the magnetization at the DW center (*blue* for positive and *red* for negative values). The hard axis is in x direction with positive *initial* chirality meaning $n_y(x_{\rm DW}, t=0) < 0$. Between $30-50$ns the chirality switches to $C=-1$ which is accompanied by an adaption to the velocity of a DW with initial negative chirality (cf. Fig. 1). Note that the magnetization is still slightly tilted towards the hard axis after switching. Parameters: $I_c = 1.0\times 10^{12}\mathrm{A/m^2}$, $\alpha_R = 0.3$.

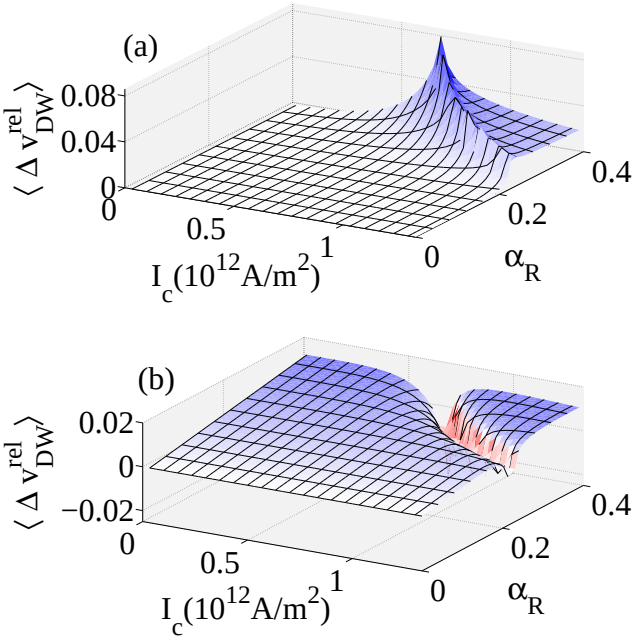

FIG. 3. (Color online) Relative difference of the average velocity $\langle \Delta v_{\rm DW}^{\rm rel}\rangle \equiv \langle v_{\rm DW}^{C=-1} - v_{\rm DW}^{C=+1}\rangle / \langle v_{\rm DW}^{C=-1} + v_{\rm DW}^{C=+1}\rangle$ for hard axis anisotropy in (a) x direction and (b) y direction. Chirality switching starts at sufficiently strong current density and Rashba coupling which is recognizable by the peaks of the velocity difference for large $I_c\alpha_R$. Red colors indicate negative and blue positive values.

entation. After the switching, the magnetizations of both initial chiralities are in the same state and thus move with equal velocity.

For a systematic understanding of the difference of the movement of the DWs with unequal initial chiralities, we plot the relative difference of the average velocities in dependence of both the current density and the Rashba coupling in Fig. 3. To do this we calculate the long term average $\langle v_{\rm DW}\rangle = x_{\rm DW}(t_{\rm end})/t_{\rm end}$ with $t_{\rm end} = 100$ns and define the relative velocity difference $\langle \Delta v_{\rm DW}^{\rm rel}\rangle \equiv \langle v_{\rm DW}^{C=-1} - v_{\rm DW}^{C=+1}\rangle / \langle v_{\rm DW}^{C=-1} + v_{\rm DW}^{C=+1}\rangle$. We find quite small velocity differences in the order of a few percents in almost the complete parameter space. In particular for a hard axis in x direction $\langle \Delta v_{\rm DW}^{\rm rel}\rangle$ is almost negligible. However, at some critical values the velocity difference is strongly increased. At these values the magnitude of the Rashba field $|\mathbf{H}_R^{\rm crit}| \approx I_c^{\rm crit}\alpha_R^{\rm crit}$ is sufficient to induce the chirality switching. The higher the Rashba field is, the earlier the switching sets in in terms of the momentary movement. Close to the critical value we only recognize the switching in our calculations if it starts at $t_{\rm switch} < t_{\rm end} = 100$ns since we only average the velocity in the time interval $t \in [0, t_{\rm end}]$. Thus, we find the largest differences when $t_{\rm switch} \approx t_{\rm end}$, as the momentary velocities of both chiralities differ up to $t_{\rm switch}$ while they match at $t > t_{\rm switch}$. Well above the critical values, the velocity difference decreases as the switching happens at an accordingly earlier time and velocities before the switching have less influence on the average.
Actually these velocity differences at $|\mathbf{H}_R| > |\mathbf{H}_R^{\rm crit}|$ would disappear in an ideal averaging process $t_{\rm end}\to\infty$, which we cannot perform since we calculate our results numerically. Nevertheless, a finite averaging, first allows us to estimate the critical parameters for a chirality switching and, second, may describe experimental results at relatively short current pulses.
Here we only show the switching from positive to negative chirality but not the opposite one. However switching to positive chirality can easily be achieved by inverting the current ($I_c \to -I_c$) which also reverses the direction of the Rashba field. Hence the chirality of a DW can be controlled by the direction of the current.

B. Suppression of the Walker breakdown

Recently Miron *et al.*[7] have found an increased DW velocity in $\mathrm{Pt/Co/AlO}_x$ wires. They argued that a spin-orbit induced field stabilizes the DW structure and suppresses a current induced Walker breakdown. We will

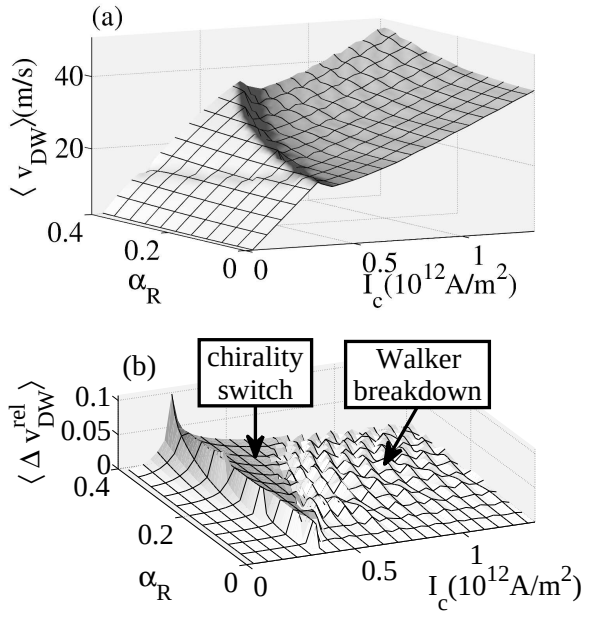

FIG. 4. DW velocities vs current density I_c and Rashba coupling α_R for a hard axis in x direction. (a): DW velocity for positive chirality. For large α_R the WB, recognizable by the local maximum of velocity at $I_c \approx 0.5 \times 10^{12}\mathrm{A/m^2}$, is shifted to higher current densities. (b) Velocity difference $\langle \Delta v_{\mathrm{DW}}^{\mathrm{rel}} \rangle = \langle v_{\mathrm{DW}}^{C=-1} - v_{\mathrm{DW}}^{C=-1} \rangle / \langle v_{\mathrm{DW}}^{C=-1} + v_{\mathrm{DW}}^{C=-1} \rangle$. In an intermediate region (the plateau denoted by "chirality switch") a single chirality switch occurs. Parameters: $\beta = 2\alpha$

investigate the effect of a Rashba interaction on the DW velocity and on the WB systematically in this section. To actually get a WB we have to choose the β parameter differently compared to the Gilbert damping α. That is why we set $\beta = 2\alpha$ below.

Indeed the WB can be shifted to higher current densities by a finite $\mathbf{H}_R$. This is shown in Fig. 4 (a). We see the typical current dependence of the DW velocity for $\alpha_R = 0$ with an large increase of the velocity below the critical current, a decrease at the WB and a moderate increase for large I_c again. As we increase the Rashba coupling this critical current density is shifted to larger values.

As it is known, a WB is accompanied by a precession of the magnetization at the DW center. This precession is suppressed by the Rashba field which favors a magnetization pointing in a distinct direction. However, as it also prefers a distinct sign of the magnetization it can induce a chirality switch [cf. Fig. 4 (b)]. This happens at a considerably lower field as for $\alpha = \beta$ (cf. Fig.3). The reason for the reduction of the critical field is quite obvious, as the system without a Rashba interaction at the WB would be already driven to a precessional dynamics by the current. Since a precession is nothing else than a frequent chirality switching, it is easy for the Rashba field to turn the magnetization to its favored direction. In other words the hard axis anisotropy has already been overcome by the current and is not felt by $\mathbf{H}_R$ anymore, which acts now as the only noticeable anisotropy. At sufficiently strong current densities, not even the combined action of $K_\perp$ and $\mathbf{H}_R$ can prevent the WB and we see small oscillations in the velocity differences in Fig. 4 (b). These stem from the precessional movement of the DW. The velocity gain of the DW due to a Rashba interaction can be up to 50% in the investigated parameter space, as shown in Fig. 5. Naturally this is in the region of the suppressed WB. We do not see major differences of the velocity neither due to the direction of the hard axis nor due to the chirality. The only remarkable difference is an increase of the velocity by increasing α_R at low current densities for a hard x axis, while it decreases in the other case.

We can conclude that in the case of $\beta > \alpha$ a WB can be shifted to higher current densities by α_R. In addition the DW's chirality can already be switched to the preferred chirality by a very small Rashba field as compared to the case of $\alpha = \beta$.

C. Short current pulses

Domain wall motion can be very sensitive on the current pulse length even in systems without a Rashba coupling[21,25,26]. Since a finite spin-orbit interaction gives rise to additional features such as chirality switching, we might expect major differences of pulsed current motion with respect to a steady current. That is why we will focus on the DW dynamics under the influence of a short current pulse in this section. A strong deviation of the movement for short pulses compared to steady motion has already be found in Ref. 21, where the Rashba field has been aligned parallel to the magnetic domains.

There are two main reasons for a deviation of averaged velocities for pulsed and steady currents. First, the momentary velocity after the start of the DW's movement can be different from the velocity at large times (cf. Fig. 1). This is even more pronounced for current densities above the WB where the velocity oscillates around an average velocity, as it can be seen in Fig. 6. For short pulses these oscillations do not cancel out in an averaging process and will strongly influence the short time average. Second, it has already been seen that the magnetization is tilted by the Rashba field out of its equilibrium position (cf. Fig. 2). When the current is turned off, the magnetic moments try to rearrange perpendicularly to the hard axis. This results in an additional movement after the pulse ("drifting", cf. Fig. 6) which has also been found in other works[7,21,27]. Depending on the tilting at the end of the pulse this drift may happen into positive or negative direction according to the movement during the pulse. The drifted distance appears to be irrelevant for long pulses, since the DW has already traveled a long distance during the pulse, but can play a major role for short pulses.

To see the effect of a non-constant movement and

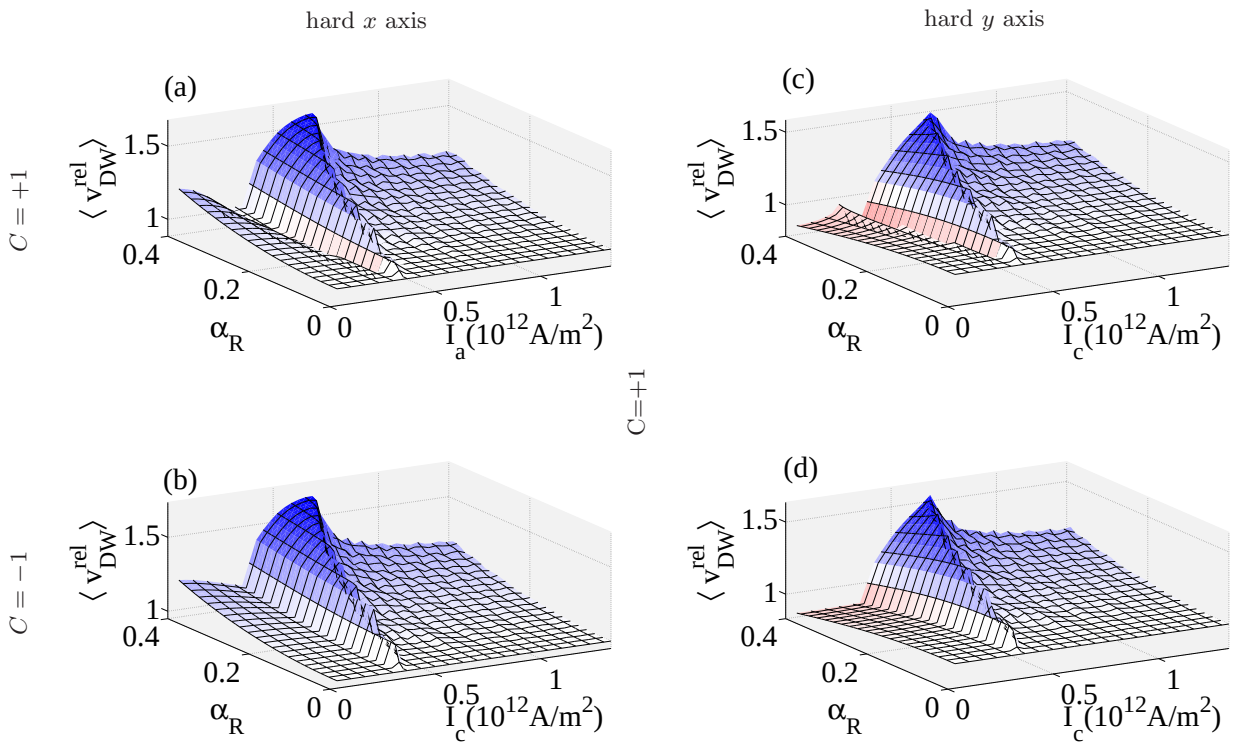

FIG. 5. (Color online) Relative DW velocity $\langle v_{\rm DW}^{\rm rel}\rangle = \langle v_{\rm DW}(\alpha_R)\rangle/\langle v_{\rm DW}(\alpha_R=0)\rangle$ Left column (a,b): hard x axis, right column (c,d): hard y axis, top panel (a,c) positive chirality and bottom panel (b,d) negative chirality. Red colors show a decrease of velocity due to the Rashba coupling, while blue ones show an increase. Here, we set $\beta = 2\alpha$

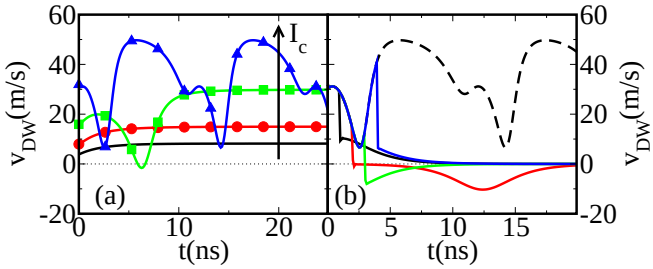

FIG. 6. (Color online) (a) Momentary DW velocity vs time for different current densities $I_c = [0.125, 0.25, 0.5, 1.0] \times 10^{12}\mathrm{A/m}^2$. (b) Momentary DW velocity vs time above the WB ($I_c = 1.0\times10^{12}\mathrm{A/m}^2$) for a steady current (dashed line) and for short current pulses of length $t_p = 1$ ns to 4 ns in steps of 1 ns. At the end of the pulse the velocity drops to a distinct finite velocity which can be either positive or negative. Thus the DW drifts a certain distance after the pulse. Parameters: $\alpha_R = 0.3$, $\beta = 2\alpha$, $C = +1$, hard x axis.

the drifting of the DW, we define two averaged velocities: (i) the average during the pulse $\langle v_{\rm DW}^{\rm pulse}\rangle(t=t_p) = x_{\rm DW}(t_p)/t_p$ and (ii) an effective average $\langle v_{\rm DW}^{\rm pulse}\rangle(t\to\infty) = x_{\rm DW}(t\to\infty)/t_p$ to include the drifting. The latter one is divided by t_p, even though we take the distance after a very long time, since it is hard to decide at which time to actually stop the averaging process as the velocity only slowly relaxes to zero.

We find that the average velocity $\langle v_{\rm DW}\rangle(t=t_p)$ during the current flow at a short pulse is typically smaller than the long time average for a steady current (cf. Fig. 7), because the momentary velocity starts at a comparably small value. But this reduction of velocity can be overcompensated by a drifting after the pulse, where the combined motion of a direct current-induced motion and drifting can appear faster than for a steady current, i.e. $\langle v_{\rm DW}^{\rm pulse}\rangle(t\to\infty) > \langle v_{\rm DW}^{\rm steady}\rangle$.

An other striking difference between $\langle v_{\rm DW}\rangle(t=t_p)$ and $\langle v_{\rm DW}^{\rm pulse}\rangle(t\to\infty)$ is the dependence on I_c. While $\langle v_{\rm DW}\rangle(t=t_p)$ as a sole short time average still shows the oscillations of the momentary velocity, the drifting, and, particularly its direction, is strongly dependent on the state of the DW magnetization (tilting) at the end of the pulse. As this tilting at t_p is either changed by the value of t_p or the current density, small deviations in these parameters can decide about the drifting direction. That is why we see sharp drops of the velocity dependence of $\langle v_{\rm DW}\rangle(t\to\infty)$ on I_c. At the drop the drift has changed from a positive to a negative direction and $\langle v_{\rm DW}\rangle(t\to\infty)$ gets smaller immediately.

For a systematic overview we plot the averaged velocity for a large parameter space in Fig. 8. As in Fig. 7 we see a smoothened velocity dependence for the average velocity during the pulse and the fast drops of $\langle v_{\rm DW}\rangle(t\to\infty)$. Since the tilting of the magnetization at a given time depends on I_c, the critical time $t_p^{(c)}$ of

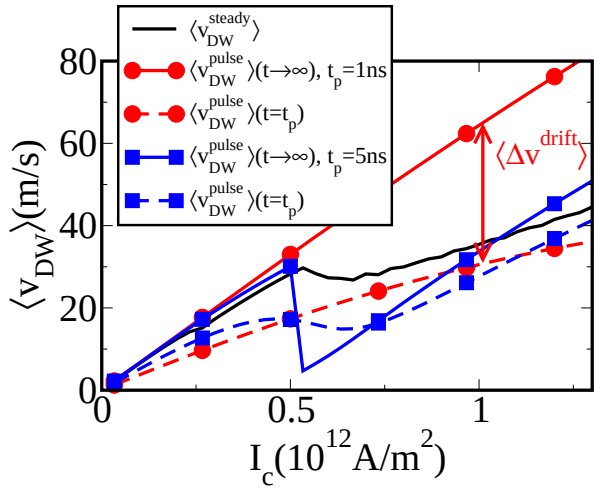

FIG. 7. (Color online) Average velocity vs current density for a steady current $\langle v_{\rm DW}^{\rm steady}\rangle$ (black, no symbols) and for a short ($t_p = 1$ ns, circles) and an intermediate ($t_p = 5$ ns, squares) pulse. For pulses the average velocity during the pulse $\langle v_{\rm DW}^{\rm pulse}\rangle(t = t_p) = x_{\rm DW}(t_p)/t_p$ (dashed lines) and the effective total velocity $\langle v_{\rm DW}^{\rm pulse}\rangle(t \to \infty) = x_{\rm DW}(t \to \infty)/t_p$ (solid lines) are given. The difference between the two respective lines represents the drifting after the pulse. Parameters: $\alpha_R = 0.3$, $\beta = 2\alpha$, $C = +1$, hard x axis.

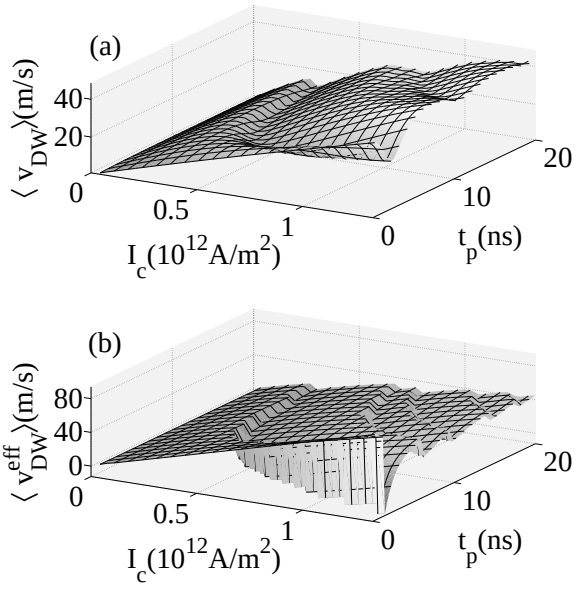

FIG. 8. DW velocities vs current density I_c and pulse length t_p. (a): Average velocity $\langle v_{\rm DW}\rangle = x_{\rm DW}(t_p)/t_p$ during the pulse. (b): Effective velocity $\langle v_{\rm DW}^{\rm eff}\rangle = x_{\rm DW}(t \to \infty)/t_p$ which includes the movement of the DW after the pulse. Both plots show results for a DW with hard axis in x direction and positive chirality. Parameters: $\alpha_R = 0.3$, $\beta = 2\alpha$.

a change of the drifting direction is also dependent on the current density. Thus the DW drifts in several directions in the investigated parameter space, which is visible in the sawtooth-like shape of the curves in Fig. 8 (b). To see the actual velocity change compared to the long-time average, we also show the relative velocity $\langle v_{\rm DW}^{\rm rel}\rangle = \langle v_{\rm DW}^{\rm pulse}\rangle(t \to \infty)/\langle v_{\rm DW}^{\rm steady}\rangle$ in Fig. 9. Here, it is possible to identify three regimes: (i) low currents, (ii) high currents and short pulses, and, (iii) high currents and comparably long pulses. For low currents, the momentary velocity at the beginning of the DW movement is smaller than the average velocity. Here, the drifting after the pulse only compensates the loss of speed during the pulse. This eventually leads to an effective velocity of the same size as the long time average. As soon as I_c is strong enough to increase the momentary velocity $v_{\rm DW}(t)$ shortly after the start of the pulse (cf. Fig. 6), $\langle v_{\rm DW}^{\rm rel}\rangle$ is also increased when there is also positive drifting, while it is decreased for negative drifting. The third regime (large I_c and t_p) comes closer to the long time averaging. In this case the drifting becomes more and more irrelevant and $\langle v_{\rm DW}^{\rm pulse}\rangle(t \to \infty)$ will settle at $\langle v_{\rm DW}^{\rm steady}\rangle$ for $t_p \to \infty$.

The aforementioned results show the important role of the additional short-time effects for the DW dynamics, in particular in presence of a spin-orbit interaction. Its experimental influence may be affected by additional phenomena not considered in this work as the presence of pinning centers[28], for instance.

IV. SUMMARY

In this paper, we have studied the influence of the direction of the hard axis and the DW chirality on the DW's current induced dynamics in 1D Rashba wires. We have calculated the spin transfer torque by a gradient expansion and solved the Landau-Lifshitz-Gilbert equation numerically. We have seen that both the chirality and the direction of the hard axis have a small effect on the DW velocity for small to intermediate values of the Rashba field $\mathbf{H}_R$. However, large Rashba fields lead to a chirality switching of the unfavored initial chirality to the preferred one at some time $t_{\rm switch}$. After the switching, the velocities of both *initial* chiralities eventually match. That is why the switching may be invisible in a long time average of the velocity, where the velocity difference before $t_{\rm switch}$ plays a minor role. As $\mathbf{H}_R$ depends approximately on the product $I_c\alpha_R$ of the current density and the Rashba coupling, the borderline of the switching in the parameter space of I_c and α_R can be estimated to $I_c^{\rm crit} \propto 1/\alpha_R^{\rm crit}$. Due to the dependence on the current density, the preferred chirality can be controlled by the direction of the current flow $I_c \to -I_c$.

Furthermore we have found a suppression of the Walker breakdown due to a finite Rashba coupling, which increases the DW velocity in the vicinity of the original ($\alpha_R = 0$) Walker breakdown. In this critical regime, it is also quite easy for the Rashba field to switch the DW's chirality as the hard axis anisotropy has been overcome by the conventional, non-Rashba, spin-transfer torque al-

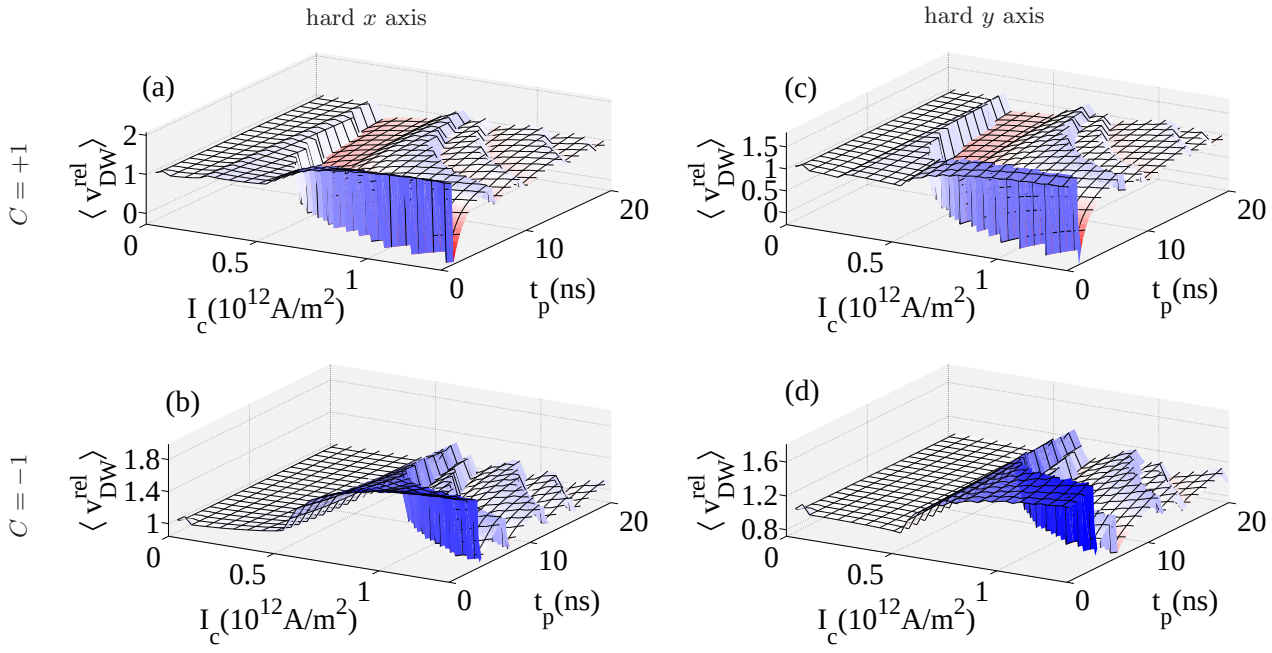

FIG. 9. (Color online) Ratio of the pulsed and steady current velocity $\langle v_{\rm DW}^{\rm rel}\rangle = \langle v_{\rm DW}^{\rm pulse}\rangle(t\to\infty)/\langle v_{\rm DW}^{\rm steady}\rangle$. Left column (a,b) hard x axis, right column (c,d) hard y axis, top panel (a,c) positive chirality and bottom panel (b,d) negative chirality. Blue values are for an increased ($\langle v_{\rm DW}^{\rm rel}\rangle > 1$) and red for a decreased pulsed velocity. Parameters: $\alpha_R = 0.3$, $\beta = 2\alpha$.

ready.

Since effects of chirality switching appear to be more pronounced in short time scales, we finally have considered short current pulses. As expected, we found a higher influence of the momentary velocity state due to a short-time averaging. More importantly, further phenomena as a drifting of the DW after a short current pulse affect the short time dynamics of a DW even more. This results partly in drastic changes of the effective DW velocity which shows a completely different dependence on the current density as compared to the steady current motion.

ACKNOWLEDGMENTS

We acknowledge support from the SFB 668 (project B16) of the DFG and thank G. Meier for valuable discussions.

[1] S. S. Parkin, M. Hayashi, and L. Thomas, Science **320**, 190 (2008).
[2] G. Malinowski, O. Boulle, and M. Kläui, J. Phys. D **44**, 384005 (2011).
[3] A. Brataas, A. D. Kent, and H. Ohno, Nature Mater. **11**, 372 (2012).
[4] A. Fert, V. Cros, and J. Sampaio, Nature Nanotech. **8**, 152 (2013).
[5] S. Zhang and Z. Li, Phys. Rev. Letters **93**, 127204 (2004).
[6] M. Hayashi, L. Thomas, C. Rettner, R. Moriya, and S. S. Parkin, Nature Phys. **3**, 21 (2006).
[7] I. M. Miron, T. Moore, H. Szambolics, L. D. Buda-Prejbeanu, S. Auffret, B. Rodmacq, S. Pizzini, J. Vogel, M. Bonfim, A. Schuhl, and G. Gaudin, Nature Mater. **10**, 419 (2011).
[8] S. Glathe, I. Berkov, T. Mikolajick, and R. Mattheis, Appl. Phys. Lett. **93**, 162505 (2008).
[9] K. Obata and G. Tatara, Phys. Rev. B **77**, 214429 (2008).
[10] A. Brataas, Nature Nanotech. **8**, 485 (2013).
[11] K.-S. Ryu, L. Thomas, S.-H. Yang, and S. Parkin, Nature Nanotech. **8**, 527 (2013).
[12] S. Emori, U. Bauer, S.-M. Ahn, E. Martinez, and G. S. Beach, Nature Mater. **12**, 611 (2013).
[13] G. Chen, T. Ma, A. T. NDiaye, H. Kwon, C. Won, Y. Wu, and A. K. Schmid, Nature Commun. **4** (2013).
[14] F. Haldane, J. Phys. C **14**, 2585 (1981).
[15] A. O. Gogolin, A. A. Nersesyan, and A. M. Tsvelik, Bosonization and strongly correlated systems (Cambridge University Press, 2004).
[16] As we will calculate the equation of motion for $\mathbf{J}_p$ later and $[\mathbf{J}_p, H_{\rm charge}]_- = 0$ the charge part will not contribute to the equation of motion.
[17] A. Schulz, A. De Martino, P. Ingenhoven, and R. Egger, Phys. Rev. B **79**, 205432 (2009).
[18] M. Thorwart and R. Egger, Phys. Rev. B **76**, 214418 (2007).
[19] E. van der Bijl and R. Duine, Phys. Rev. B **86**, 094406 (2012).

[20] K.-W. Kim, S.-M. Seo, J. Ryu, K.-J. Lee, and H.-W. Lee, Phys. Rev. B **85**, 180404 (2012).
[21] M. Stier, R. Egger, and M. Thorwart, Phys. Rev. B **87**, 184415 (2013).
[22] M. Hayashi, Y. Nakatani, S. Fukami, M. Yamanouchi, S. Mitani, and H. Ohno, J. Phys. Condens. Matter **24**, 024221 (2012).
[23] J. Linder, Phys. Rev. B **87**, 054434 (2013).
[24] J. Otálora, J. López-López, P. Landeros, P. Vargas, and A. Núñez, J. Magn. Magn. Mater. **341**, 86 (2013).
[25] L. Thomas, M. Hayashi, X. Jiang, R. Moriya, C. Rettner, and S. S. Parkin, Nature **443**, 197 (2006).
[26] G. Meier, M. Bolte, R. Eiselt, B. Krüger, D.-H. Kim, and P. Fischer, Phys. Rev. Lett. **98**, 187202 (2007).
[27] L. Thomas, R. Moriya, C. Rettner, and S. S. Parkin, Science **330**, 1810 (2010).
[28] B. Van de Wiele, L. Laurson, and G. Durin, Eur. Phys. J. B **86**, 1 (2013).